Neurochemical Research (2021) 46:455–467
https://doi.org/10.1007/s11064-020-03179-9

ORIGINAL PAPER

Mechanism of Human Umbilical Cord Mesenchymal Stem Cells Derived-Extracellular Vesicle in Cerebral Ischemia-Reperfusion Injury

Wenlei Wang[1] · Zhen Ji[1] · Chunyan Yuan[2] · Yanfang Yang[1]

Received: 4 March 2020 / Revised: 9 November 2020 / Accepted: 11 November 2020 / Published online: 30 November 2020

Abstract

Mesenchymal stem cells (MSCs)-derived extracellular vesicles (EVs) are implicated in cerebral ischemia reperfusion (I/R) injury process. In this study, after extraction and identification of human umbilical cord MSCs (HMCs)-derived EVs, I/R rat models were established and treated with HMC-EVs to measure pathological damage, apoptosis and inflammation in brain tissues. The differentially expressed microRNAs (miRs) in HMC-EVs and I/R rat tissues were screened. The downstream gene and pathways of miR-24 were analyzed. The gain- and loss-of function of miR-24 in HMC-EVs was performed in I/R rat models and hypoxia/reoxygenation (H/R) cell models. SH-SY5Y cells were subjected to hypoxia and biological behaviors were detected by MTT assay, colony formation experiment, EdU staining and Transwell assays, and cells were incubated with the inhibitors of downstream pathways. As expected, infarct size, brain tissue apoptosis and inflammation were decreased after HMC-EVs treatment. miR-24 overexpression in HMC-EVs reduced I/R injury, while miR-24 knockdown in HMC-EVs impaired the protective roles of HMC-EVs in I/R injury. HMC-EVs-carried miR-24 could target AQP4 to activate the P38 MAPK/ERK1/2/P13K/AKT pathway, and thus promoted the proliferation and migration of SH-SY5Y cells after H/R injury, which were reversed by LY294002 and PD98095. Taken together, HMC-EVs-carried miR-24 played protective roles in I/R injury, possibly by targeting AQP4 and activating the P38 MAPK/ERK1/2/P13K/AKT pathway. This study may offer novel perspective for I/R injury treatment.

Keywords Cerebral ischemia reperfusion injury · Human umbilical cord mesenchymal stem cells · Extracellular vesicles · microRNA-24 · AQP4 · P38 MAPK/ERK1/2

Introduction

Ischemia means the lack of blood supply for tissues owing to the obstruction of arterial inflow, while reperfusion, although essential to reconstruct the delivery of oxygen and nutrients to normalize cell metabolism, it may cause the pathogenic process, aggravate the damage caused by ischemia itself, and result in tissue damage in distant organs [1]. When cerebral blood flow is interrupted transiently, cerebral ischemia/reperfusion (I/R) injury occurs following oxygen and glucose deprivation. The resulting brain dysfunction leads to high rates of mortality and disability [2]. I/R injury is related to severe clinical manifestations, such as myocardial hibernation, cerebral disorder, acute heart failure, gastrointestinal disorder, systemic inflammatory response, and multiple organ impairment [3]. Unfortunately, there is still a long way to go before the establishment of brain protection strategy or the successful enhancement of the mechanism of post ischemic repair [4]. Besides, studies have indicated mesenchymal stem cells (MSCs) are appealing in regenerative medicines due to their abilities of self-renewal and regeneration of damaged tissues, as well as functions in regulating inflammation, autoimmune and organ injury [5, 6]. Furthermore, MSCs-derived extracellular vesicles (EVs) attenuated lung IRI and promoted donor lung repair after circulatory failure [7]. In light of these discoveries, this study tries to find novel approaches for cerebral I/R injury from the aspect of MSCs-derived EVs.

✉ Yanfang Yang
yangyf_1026@163.com

[1] Department of Neurology, Qingdao Chengyang People's Hospital, No. 600 Changcheng Road, Chengyang District, Qingdao 266109, Shandong, People's Republic of China

[2] Department of Rehabilitation Medicine, Qingdao Chengyang People's Hospital, Qingdao 266109, Shandong, People's Republic of China

Human umbilical cord MSCs (HMCs) are widely used in regeneration, and their roles in alleviating liver fibrosis, promoting liver and renal injury recovery, and facilitating wound healing have been found [8]. HMCs have also been reported to relieve hyperemia and inflammation, and to meliorate I/R-induced acute renal failure in rats [9]. Additionally, stem cells can communicate with adjacent cells and remote cells through EVs, and stem cell-derived EVs carrying certain proteins and RNAs can support healing of injured tissues [10]. Besides, EVs released by MSCs could alleviate I/R-induced inflammation and renal injury [11]. Furthermore, EVs, transferring mRNAs and microRNAs (miRs) to target cells, are key regulators of cell-cell communication, and circulating EVs monitor tissue regeneration and remote ischemic preconditioning [12, 13]. A variety of miRs have been uncovered in different organs after I/R to regulate gene functions in cardiomyocyte death, fibrosis, extracellular matrix remodeling, inflammatory response and angiogenesis [14]. The abovementioned demonstrations triggered us to screen out the differentially expressed miR in HMC-EVs and rat tissues with I/R injury, as well as the potential downstream genes and pathways. Thereby, this study was designed to evaluate the underlying molecular mechanism of HMC-EVs on cerebral I/R injury in vivo and in vitro.

Materials and Methods

Isolation and Identification of HMCs

The cord tissues provided by Affiliated Hospital of Jiangsu University (Zhenjiang, Jiangsu, China) were cultured in low-glucose Dulbecco' s modified Eagle medium (L-DMEM, Gibco, Grand Island, NY, USA) containing 10% fetal bovine serum (FBS). When cell confluency reached 80%, cells were detached using trypsin and subculture.

The HMCs of the third passage were obtained, and the expression of cell surface markers CD105, CD29, CD44 and CD34 was detected using flow cytometer (Beckman Coulter, Inc., Chaska, MN, USA). Adipocyte induction medium and osteoblast induction medium (Gibco) were used to induce HMCs to differentiate into adipocytes and osteoblasts, respectively. Oil red O staining and alizarin red staining were used to observe the adipogenesis and osteogenesis.

Isolation, Identification and Treatment of HMC-EVs

EVs were extracted from HMC supernatant by ultracentrifugation [15]. The morphology of EVs was observed under the transmission electron microscope (TEM) (Olympus, Tokyo, Japan). The size and distribution of EV samples were observed by nanoparticle tracking analysis (NTA). The expression of CD9, CD63, Alix 3 and Cis-Golgi matrix 130 (GM130) on the EV surface was detected by western blot analysis.

HMCs were seeded into 6-well plates at 1×10^4cells/well. On the next day, HMCs were transfected with miR-24 mimic/inhibitor/negative control (NC) (Shanghai Genechem Co., Ltd., Shanghai, China) according to the instructions of Lipofectamine™ 2000 kit (Invitrogen Inc., Carlsbad, CA, USA), and the final concentration was 100 nmol/L. After 48 h of transfection, the EVs were extracted for further experiments.

Establishment and Grouping of Rat Models with I/R

A total of 119 male Sprague Dawley rats (280 ± 20 g) were purchased from Zhejiang Vital River Laboratory Animal Technology Co., Ltd. (Jiaxing, Zhejiang, China, SCXK (Zhejiang) 2018–0001). Seventeen rats enrolled in the sham group only had the right carotid artery separated, and the remaining 102 rats were used for I/R modeling using the suture-occluded method [16]. Briefly, after midline incision in the neck skin, the right external carotid artery (ECA) was isolated from the surrounding nerves and fascia. A nylon suture of 0.26 mm diameter was introduced into the ECA and went on into the internal carotid artery to obstruct the right ECA. The suture was inserted 18–20 mm from the bifurcation of the common carotid artery. The rectal temperature of rats was maintained at 37 ± 0.5 °C during the operation. After awakening, neurological deficits were evaluated as previously described [17]. Rats without left forelimb paresis or circling towards the left side were considered as unsuccessful models and were excluded. The rats were anesthetized with ether 90 min after middle cerebral artery occlusion modeling and the suture was withdrawn. No rats died in the process of modeling.

I/R rats (all successfully modeled) were then allocated into 6 groups, with 17 rats in each group. Specifically, during reperfusion, rats in the I/R group were injected with 2 mL phosphate buffer saline (PBS); rats in the HMC-EV group were injected with 100 μg HMC-ex via the tail vein for 3 consecutive days, 100 μg per day; rats in the NC/HMC-EV group were injected with 100 μg NC/HMC-EVs via the tail vein for 3 consecutive days, 100 μg per day; rats in the miR-24/HMC-EV group were injected with 100 μg miR-24/HMC-EVs via the tail vein for 3 consecutive days, 100 μg per day; rats in the in-NC/HMC-EV group were injected with 100 μg in-NC/HMC-EV via the tail vein for 3 consecutive days, 100 μg per day; rats in the in-miR-24/HMC-EV group were injected with 100 μg miR-24 inhibitor/HMC-EV via the tail vein for 3 consecutive days, 100 μg per day. After 24 h of the last injection, in each group, brain tissues of 5 rats were taken to prepare tissue homogenate, 6 rats were used for triphenyl tetrazolium chloride (TTC) staining, 6 rats were used for hematoxylin and eosin (HE) staining, terminal

deoxynucleotidyl transferase (TdT)-mediated dUTP nick end labeling (TUNEL) and immunohistochemistry.

TTC Staining

Rats were deeply anesthetized using 30 mg/kg pentobarbital sodium to quickly obtain the brains. Then brain tissues were frozen in the refrigerator at −20 °C for 18 min, and then taken out and cut into 6 sections at 2 mm along the coronal plane of brain tissues. Afterwards, the brain sections were placed in 2% TTC solution (Sigma-Aldrich, Merck KGaA, Darmstadt, Germany) at 37 °C for 30 min without light exposure. Later, the sections were fixed in 4% paraformaldehyde and photographed using a digital camera, and then the infarct size was calculated by Image J software (National Institutes of Health, Bethesda, Maryland, USA).

HE Staining

After model establishment, pentobarbital sodium was injected into rats for deep anesthesia, and the brains were taken and fixed in 10% neutral formalin solution for 48 h. After alcohol gradient dehydration, xylene soaking, wax immersion and embedding, the waxed blocks were sliced at 3 μm. Brain sections were stained with hematoxylin, differentiated with 75% ethanol hydrochloride, and counterstained with eosin. Afterwards, the morphology of brain tissues was observed under a microscope (Olympus).

TUNEL Assay

Brain sections of rats were taken for detecting apoptotic index using the TUNEL method as per the instructions of the kit (Boster Biological Technology Co., Ltd., Wuhan, Hubei, China). Results were presented as the apoptosis index (AI), the ratio of TUNEL-positive cells (brown cells) to total cells in the same field of view [18].

Immunohistochemistry

The prepared brain sections were used for immunohistochemistry using Streptavidin-Biotin Complex methods by incubation with B cell lymphoma-2 (Bcl-2) (1:250, ab32124). For semi-quantitative analyses, areas of positive staining were defined by two independent investigators using Image-Pro 6.0 Plus (Media Cybernetics). Five fields of view for each section were randomly selected, images were acquired, and integrated optical density (IOD) was determined [density (mean) = IOD/area] [18].

Enzyme-Linked Immunosorbent Assay (ELISA)

The levels of inflammatory factors in brain tissue homogenate were detected according to interleukin-6 (IL-6) and tumor necrosis factor-α (TNF-α) detection kits (Shanghai Bohu Biotechnology Co., Ltd., Shanghai, China).

Microarray Analysis

The brain tissues of the modeled rats with or without EV injection were used for microarray analysis, which was carried out by Shanghai Sensichip Hightech Co., Ltd. (Shanghai, China). Total RNA 50 μg was used for separation and purification of miRs by polyethylene glycol (PEG) method. Using T4 RNA ligase labeling method, miR was labeled with fluorescence, then precipitated with anhydrous ethanol, dried and dissolved in 16 μL hybridizing solution, and hybridized overnight at 42 °C. At the end of hybridization, the samples were washed in a solution containing 0.2% SDS and 2 × SSC (2 × saline sodium citrate, diluted from 20 × SSC, which was composed of 3.0 M NaCl and 0.3 M Na_3citrate·$2H_2O$, PH7.0) at 42 °C for 4 min, and then washed in 0.2 × SSC at room temperature for 4 min. After the slide was dried, it was scanned with LuxS-can 10 K/A dual-channel laser scanner, and the operation was repeated twice in each sample. LuxScan3.0 image analysis software (CapitalBio company) was used to analyze the chip image. After the overall normalization and logarithmic transformation of the data, the differentially expressed genes were selected by means of signature analysis of microarrays (SAM, version 2.1). The screening criteria were as follows: false discovery rate (FDR) was controlled within 5%, and fold change was not less than 2.0. Finally, Cluster 3.0 (Stanford University) was used for cluster analysis.

Reverse Transcription Quantitative Polymerase Chain Reaction (RT-qPCR)

Total RNA was obtained from rat brain homogenate and SH-SY5Y cells using the one-step method of Trizol (Invitrogen) to determine its concentration and purity, reversely transcribed into cDNA, and then amplified using PCR instrument. The mRNA expression of primers in Table 1 was detected by SYBR PCR Master Mix Kit (Thermo Fisher Scientific Inc., Waltham, MA, USA) with U6 or β-actin as internal references. The primers used in the experiment were designed by Primer 3Plus website and synthesized by Suzhou Genewiz Bio-engineering Co., Ltd. (Suzhou, Jiangsu, China). The experiment was repeated for 3 times.

Table 1 Primer sequences of RT-qPCR

Primer	Sequence (5′ → 3′)
miR-24	F: GACTCCTGTTCCTGCTGAACT
	R: GTTGTTCCAGGCTGTTGATGG
U6	F: CTCGCTTCGGCAGCACA
	R: GTGTCGTGGAGTCGGCAA
AQP4	F: CCTGCCATCTTCGGGTACTG
	R: GCCATTTCAAAGCAATCAAATGCAA
β-actin	F: GTCATTCCAAATATGAGAGATGCGT
	R: GCTATCACCTCCCCTGTGTG

RT-qPCR reverse transcription quantitative polymerase chain reaction, *miR-24* microRNA-24, *AQP4* aquaporin 4, *F* forward, *R* reverse

Table 2 Antibodies used in western blot analysis

Antibody	Item no	Dilution ratio	Company
GM130	ab52649	1:1000	Abcam
CD9	ab92726	1:2000	Abcam
CD63	ab134045	1:1000	Abcam
Alix3	ab117600	1:1000	Abcam
AQP4	ab46182	1:1000	Abcam
p-MAPK	4511	1:1000	CST
MAPK	8690	1:1000	CST
p-ERK1/2	4370	1:2000	CST
ERK1/2	ab17942	1:1000	Abcam
PI3K	4292	1:1000	CST
p-PI3K	ab182651	1:500	Abcam
AKT	ab179463	1:10000	Abcam
p-AKT	ab38449	1:1000	Abcam
cleaved caspase-3	ab49822	1:500	Abcam
β-actin	ab64946	1:1000	Abcam

AQP4 aquaporin 4, *MAPK* mitogen-activated protein kinase, *ERK* extracellular signal-regulated kinase, *PI3K* phosphatidyl inositol 3-kinase, *AKT* protein kinase B

Western Blot Analysis

Rat brain homogenate and SH-SY5Y cells were lysed with radio-immunoprecipitation assay lysis buffer (50 mM Tris-HCl (PH7.5), 150 mM NaCl, 1% NP-40, 0.1% SDS, 0.5% sodium deoxycholate, 5 mM EDTA, 0.1 mM PMSF, 2 mg/mL aprotinin, 5 mM NaF and 2 mM NaVO3). The proteins were extracted and quantified using the bicinchoninic acid (BCA) method. The proteins were run on polyacrylamide gel electrophoresis, and transferred to membranes at constant 90 mA. After that, the membranes were sealed with 50 g/L milk for 1 h, and incubated with primary antibodies (Table 2) overnight. On the next day, the membranes were incubated with horseradish peroxidase-labeled secondary antibody goat anti-rabbit immunoglobulin G (ab6728, 1:2000) or goat anti-mouse IgG (ab205719, 1:2000), and visualized with enhanced chemiluminescence reagent. Bio-Rad Digital Image System (Bio-Rad Laboratories, Inc. Hercules, CA, USA) was applied to analyze the results.

Establishment and Grouping of Hypoxia/reoxygenation (H/R)-Treated Cell Models

SH-SY5Y cells (purchased from Nanjing Cobioer Biotechnology Co., Ltd., Nanjing, Jiangsu, China) were seeded in culture dishes and then placed into an AnaeroPack box (Mitsubishi Gas Chemical America, Inc., New York, USA) for 0–8 h to mimic the hypoxia process. Subsequently, culture media were replaced with DMEM containing 10% FBS for 24-h cultivation.

After H/R treatment for 6 or 24 h, SH-SY5Y cells were assigned into 7 groups during reoxygenation. In brief, cells in the H/R group were added with PBS; cells in the H/R + NC/HMC-EV group were added with 10 μL NC/HMC-EV; cells in the H/R + miR-24/HMC-EV group were added with 10 μL miR-24/HMC-EV; cells in the H/R + miR-24/HMC-EV + LY294002 and PD98095 (Sigma-Aldrich) group were added with 10 μL miR-24/HMC-EV, and 20 μM LY294002 and PD98095; cells in the H/R + in-NC/HMC-EV group were added with 10 μL in-NC/HMC-EV; and cells in the H/R + in-miR-24/HMC-EV group were added with 10 μL in-miR-24/HMC-EV.

3-(4, 5-Dimethylthiazol-2-yl)-2, 5-diphenyltetrazolium bromide (MTT) Assay

Cells were seeded into 96-well plates at 150 μL/well with the density of 3×10^5 cells/mL, and then each well was added with 15 μL MTT solution at 37 °C for 2 h when culturing for 0 h, 24 h, 48 h and 72 h. Following media removal, each well was added with 10 μL dimethyl sulphoxide solution. The optical density value at 450 nm was determined using a microplate reader (Bio-Rad Laboratories).

Colony Formation Assay

The cells of each group in logarithmic growth phase were seeded into 6-well plates. When there were visible colonies in the culture plates, the cultivation was terminated. After that, cells were fixed with 1 mL 4% paraformaldehyde for 15 min, and then stained with 1 mL 0.5% crystal violet Esolution for 30 min. The 6-well plates were observed under the microscope (Olympus) to count the colony numbers which had over 50 cells.

5-Ethynyl-2′-deoxyuridine (EdU) Labeling Assay

Cell proliferation was detected by BeyoClick™ EdU kit (Beyotime Biotechnology Co., Ltd., Shanghai, China) [19].

Flow Cytometry

Cells seeded into the 6-well plates were made into 1×10^5/mL cell suspension. After that, cell suspension was incubated with 5 μL Annexin V-fluorescein isothiocyanate (MultiSciences (Lianke) Biotechnology Corporate Limited, Hangzhou, Zhejiang, China) for 10 min without light exposure. Then cells were resuspended and cultured with 5 μL propidium iodide for 20 min, followed by apoptosis detection on the flow cytometer (Thermo Fisher Scientific Inc.).

Transwell Assay

Matrigel (100 μL) was evenly coated on the apical chamber of Transwell (no such step in cell migration experiment). Then cells in each group were seeded in the apical chamber at 100 μL/well with the density of 1×10^5 cells/mL. Each basolateral chamber was covered with 500 μL 10% FBS and the Transwell chambers were cultured in the medium for 24 h. After that, cells which did not cross the membrane in the apical chamber were wiped off with cotton swabs. Cells crossing the membrane were fixed with 4% paraformaldehyde at room temperature for 30 min, and stained with 0.5% crystal violet (Beyotime). Following 3 PBS washes (each for 5 min), cells in randomly selected 5 fields of vision were observed, photographed and counted under a microscope (Olympus).

Dual Luciferase Reporter Gene Assay

The 3′ untranslated region (3′UTR) sequence of aquaporin 4 (AQP4) containing the binding site of miR-24 was synthesized, and the wild type (WT) plasmid (AQP4-WT) and mutant type (MUT) plasmid (AQP4-MUT) of AQP4 3'UTR were constructed. The constructed plasmids were mixed with NC and miR-24 plasmids respectively and then transfected into HEK293 cells (American Type Culture Collection, ATCC, Manassas, Virginia, USA). Afterwards, cells were collected and lysed after transfection for 48 h. Luciferase activity was detected by Luciferase Detection Kit (BioVision, San Francisco, CA, USA) and Glomax 20/20 luminometer (Promega, Madison, Wisconsin, USA).

Statistical Analysis

Statistical analysis was conducted by SPSS21.0 (IBM Corp. Armonk, NY, USA). Kolmogorov-Smirnov test checked whether the data were normally distributed. The measurement data were exhibited in mean ± standard deviation. The *t* test was applied for comparisons between two groups, while one-way or two-way analysis of variance (ANOVA) for multi-groups and Tukey's multiple comparisons test for pair-wise comparisons after ANOVA analyses. The *p* value was obtained by two-tailed tests and $p < 0.05$ meant statistical differences.

Results

Identification of HMC and HMC-EVs

The long-fusiform, uniform and fibroblast-like cells could be observed after 10 days of adherent culture of human umbilical cord tissue blocks. About 2 weeks later, when cell confluency reached 80%–90%, cells were passaged till P3 generation for subsequent identification and biological experiments (Fig. 1a). In the process of osteogenic differentiation, HMCs changed from long-fusiform to irregular shapes and distributed in "wedge" shapes. With the induction time going, the cell structure gradually disappeared, cells gradually fused, and calcium deposition appeared. On the 14th day after induction, the osteoblasts were identified by alkaline-phosphatase staining. Under the microscope, the precipitates in the cytoplasm were red (Fig. 1b). After 3 weeks of adipogenic induction, oil red O staining was used to observe the adipogenic differentiation. Under the microscope, HMCs increased in volume, irregular in shape, and multiple round orange red lipid droplets with different sizes appeared in the cytoplasm (Fig. 1c). These results indicated that the cultured cells had the characteristics of multidirectional differentiation of MSCs. Flow cytometry was then used to detect the expression of cell surface markers. The results exhibited that the cell surface antigen CD34 was negative, while CD105, CD29 and CD44 were positive, meeting the international criteria for MSCs (Fig. 1d). In conclusion, HMCs were successfully isolated and cultured.

After HMCs were successfully extracted, EVs from HMCs were obtained by ultracentrifugation and identified by TEM, NTA and western blot analysis. EVs was in 30–100 nm diameter, in round or quasi round, presenting in microcapsules like saucers wrapped in lipid membranes (Fig. 1e). The size of the microcapsules was different (Fig. 1f). According to the definition of MISEV 2018 revision, they belong to small EVs [20]. Besides,

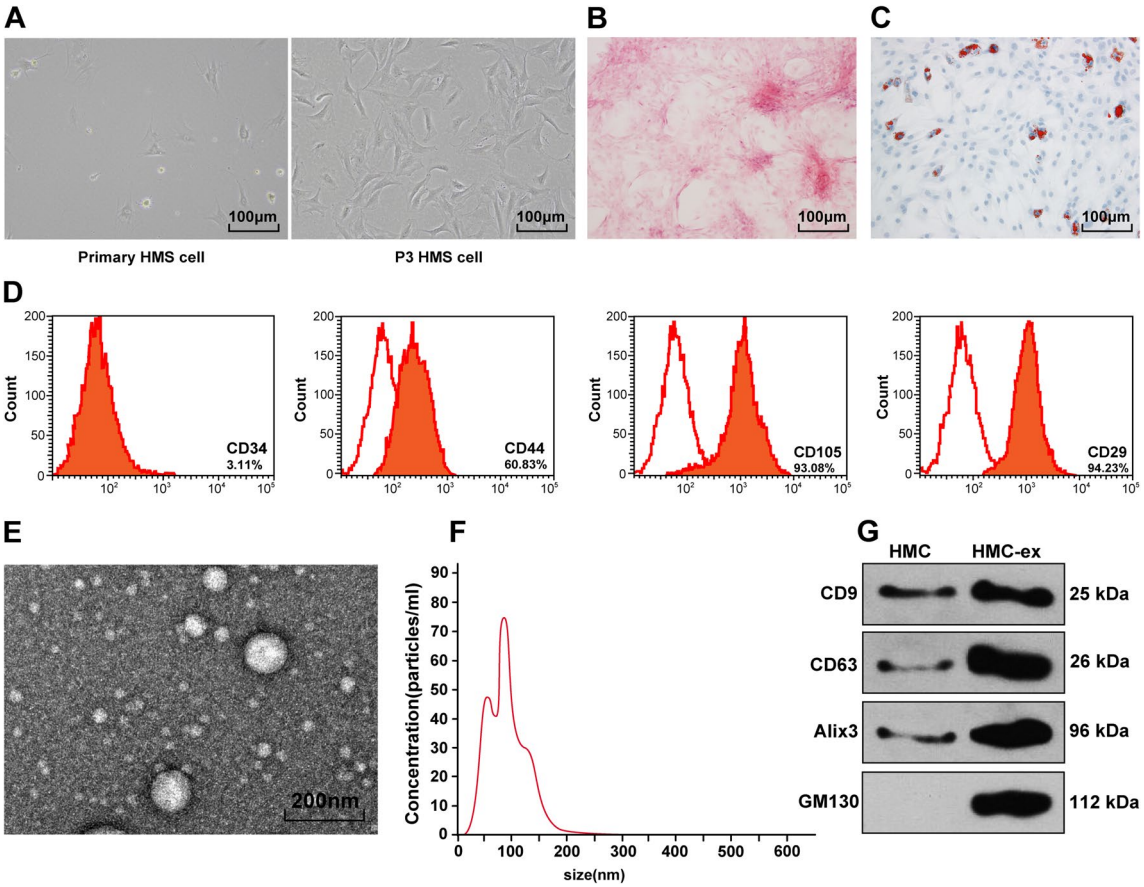

Fig. 1 HMCs and HMC-EV are successfully obtained. (**a**) Morphology of primary HMCs and HMCs at P3 generation; (**b**) Cell adipogenesis was induced and the precipitates in the cytoplasm were red observed by alizarin red staining; (**c**) HMCs increased in volume, irregular in shape, and multiple round orange red lipid droplets with different sizes appeared in the cytoplasm observed by oil red O staining; (**d**) Flow cytometry detected the expression of cell surface markers, showing that CD34 was negative, while CD105, CD29 and CD44 were positive; (**e**) Morphology of extracted HMC-EV observed by TEM, showing that EV diameter was between 30 and 100 nm, in round or quasi round; (**f**) NTA measured that particle size of HMC-EV was 40 ~ 100 nm, and the peak value was at 80 nm; (**g**) Western blot analysis measured HMC-EV surface markers GM130, CD9, CD63 and Alix3, showing that CD9, CD63 and Alix3 were overexpressed, but GM130 was not expressed

EV surface marker proteins CD9, CD63 and Alix3 were overexpressed, but GM130 was not expressed (Fig. 1g), indicating the successful extraction of HMC-EVs.

HMC-EVs are Protective for Cerebral I/R Injury

It has been reported that plasma Evs could protect the myocardium from I/R injury [21]. To investigate the effect of HMC-EV on cerebral I/R injury, we successfully established I/R models in the right middle cerebral artery of rats, and detected the degree of cerebral infarction 24 h after reperfusion. The results of TTC staining showed that the volume of infarct size decreased significantly after EV treatment (Fig. 2a). The results of HE staining showed that the cortex of rats in the sham group was complete without obvious apoptosis, while the atrophy and apoptosis degree of cells in the rats with cerebral I/R injury were more serious than those in the EV treatment group (Fig. 2b). Additionally, TUNEL staining and immunohistochemistry were performed to evaluate apoptosis of brain tissues in rats. The results showed that the number of TUNEL-positive cells and cleaved caspase3 expression in the brain tissues of rats treated with EVs were significantly lower than those in rats with cerebral I/R injury, and Bcl-2 expression was significantly higher than that in rats with cerebral I/R injury (all $p < 0.05$) (Fig. 2c–e). In addition, we also detected the levels of IL-6 and TNF-α in brain tissues of rats in each group. The results showed that levels of IL-6 and TNF-α in brain tissues of rats treated with HMC-EVs were significantly lower than those without HMC-EV treatment (Fig. 2f) (all $p < 0.01$). Based on the above results, we could conclude that HMC-EVs have a certain protective effect on rats with cerebral I/R injury.

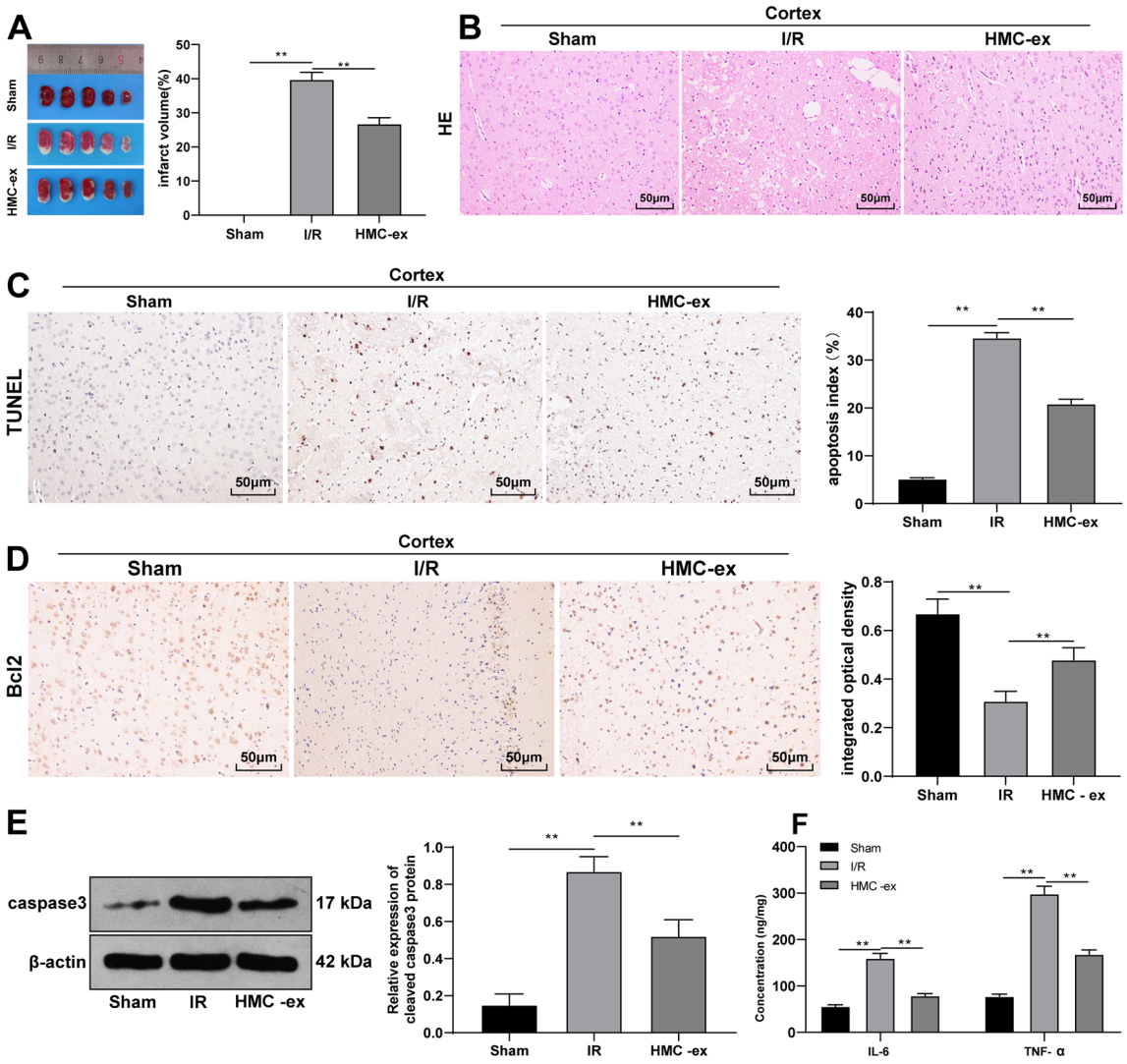

Fig. 2 HMC-EV has protective effects on rats with cerebral I/R injury. (**a**) TTC staining showed that the volume of infarct size decreased significantly after HMC-EV treatment, with white area presenting ischemic infarct area ($n=6$); (**b**) HE staining was used to detect the pathological morphology of the cortex in each group (n = 6); (**c**) TUNEL staining observed the number of TUNEL-positive cells in the cortex of rats in each group, with brown cells representing apoptotic cells (n = 6); (**d**) The expression of cleaved caspase3 and Bcl-2 in the cortex of rats was detected by immunohistochemistry (n = 6); (**e**) The expression of cleaved caspase3 in the cortex of rats was detected by western blot analysis ($n=5$, the experiment was repeated three times); (**f**) The expression of IL-6 and TNF-α in brain tissues of rats was detected by ELIKA kits ($n=5$). The experiments were performed 3 times. $^*p<0.01$. Data in panels **a**, **c**, **d** and **e** were analyzed by one-way ANOVA, and data in panel **f** were analyzed by two-way ANOVA. Tukey's multiple comparisons test was used for pairwise comparison after ANOVA

HMC-EVs Mitigate Cerebral I/R Injury by Releasing miR-24

RNA in EVs can shuttle between cells and participate in the regulation of gene expression in receptor cells [22]. Therefore, we speculated that the protective effect of HMC-ex on cerebral I/R injury may also be related to miR cargo. To test this hypothesis, we used microarray to analyze the differentially expressed miRs in the brain tissues between I/R rats with or without EV injection. The results showed that there were multiple differentially expressed miRs between the two groups, and miR-24 has a very significant difference ($p<0.05$) (Fig. 3a). Therefore, we speculate that HMC-EVs may carry miR-24 and release it into the brain tissues of rats, thus protecting the brain from cerebral I/R injury. To confirm this hypothesis, we successfully transfected miR-24 mimic/inhibitor into HMCs (Fig. 3b), and extracted their EVs and injected them into rats via the tail veins. TTC staining and HE staining were used for pathological morphological evaluation, TUNEL staining, western blot analysis and

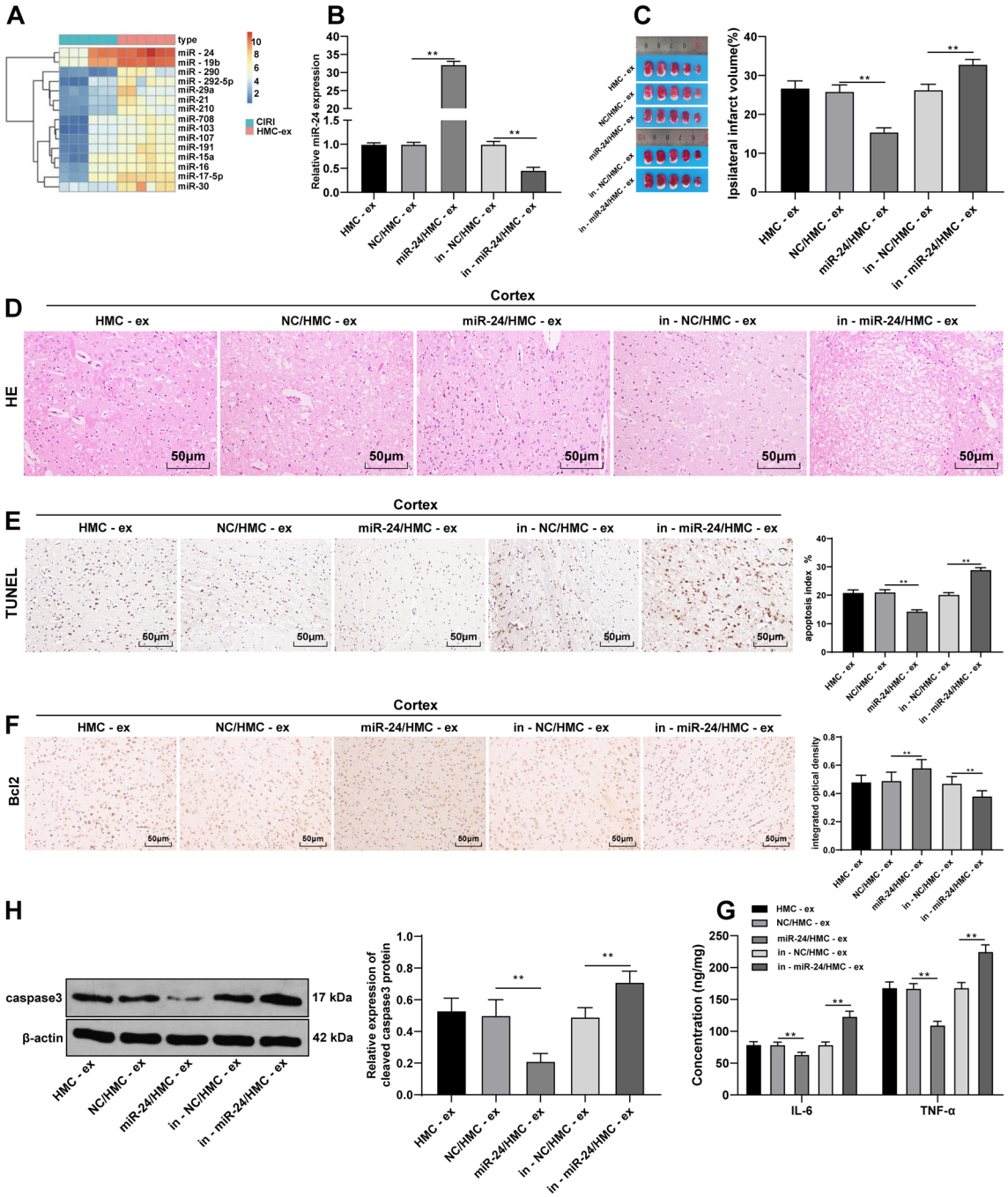

Fig. 3 HMC-EV mitigates cerebral I/R injury by releasing miR-24. (**a**) Microarray analyzed the differentially expressed miRs in the brain tissues of I/R rats and rats injected with HMC-EV. The results showed that there were multiple differentially expressed miRs in the two groups, and miR-24 has a very significant difference (n = 5); (**b**) The transfection efficiency of miR-24 mimic/inhibitor was verified by RT-qPCR (n = 5); (**c**) TTC staining detected infarct size with white area presenting ischemic infarct area (n = 6); (**d**) HE staining detected the pathological morphology of the cortex in each group (n = 6); (**e**) TUNEL staining observed the number of TUNEL-positive cells in the cortex of rats in each group, with brown cells representing apoptotic cells (n = 6); (**f**) The expression of cleaved caspase3 and Bcl-2 in brain tissues of rats were detected by immunohistochemistry, with brown cells representing apoptotic cells (n = 6); (**g**) The expression of cleaved caspase3 in the cortex of rats was detected by western blot analysis (n = 5, the experiment was repeated three times); (**h**) The expression of IL-6 and TNF-α in brain tissues of rats were detected by ELIKA kits (n = 5). The experiments were performed 3 times. *$p < 0.01$. Data in panels **b**, **c**, **e**, **f** and **g** were analyzed by one-way ANOVA, and data in panel H were analyzed by two-way ANOVA. Tukey's multiple comparisons test was used for pairwise comparison after ANOVA

immunohistochemistry were used to detect the apoptosis of brain tissues, and ELISA detected inflammatory factors in brain tissues. The results showed that the protective effect of HMC-EVs with overexpressing miR-24 on cerebral I/R injury was enhanced, while that of HMC-EVs with low expressing miR-24 was decreased (Fig. 3c–h).

miR-24 Targets AQP4 to Activate the P38 MAPK/ERK1/2/P13K/AKT Axis

In the above results, we confirmed that HMC-EVs releases miR-24 to alleviate cerebral I/R injury, but the downstream mechanism is still unclear. Through a reference review, we found that AQP4 knockout can reduce oxygen-glucose deprivation-induced astrocyte injury [23]. It was predicted that the AQP4 is one of the target genes of miR-24 through the biological website. The dual luciferase reporter gene assay precisely verified that there is a binding region between miR-24 and AQP4. After miR-24 overexpression in HMC-EVs, AQP4 levels were significantly reduced, which were opposite when miR-24 expression in HMC-EVs was knocked down (Fig. 4a–c) (all $p < 0.05$). Besides, P38 MAPK/ERK1/2 and PI3K/AKT are important signaling pathways involved in the regulation of cell apoptosis after stroke [24]. Therefore, western blot analysis was used to detect levels of P38 MAPK/ERK1/2/P13K/AKT signaling pathway-related proteins in the brain tissues of each rat. It was found that HMC-EVs with overexpressing miR-24 activated the MAPK/ERK1/2/P13K/AKT signaling pathway (Fig. 4d–e). In summary, we confirmed that miR-24 released from HMC-EVs inhibited AQP4 expression, activated the P38 MAPK/ERK1/2/P13K/AKT signaling pathway, and thus protecting rats from cerebral I/R injury.

HMC-EVs-Carried miR-24 Restores SH-SY5Y Cell Proliferation and Migration After H/R

We have explored the mechanism of HMC-EVs in rats with cerebral I/R injury through in vivo experiments. However, its effect in vitro remained unclear. Therefore, we established

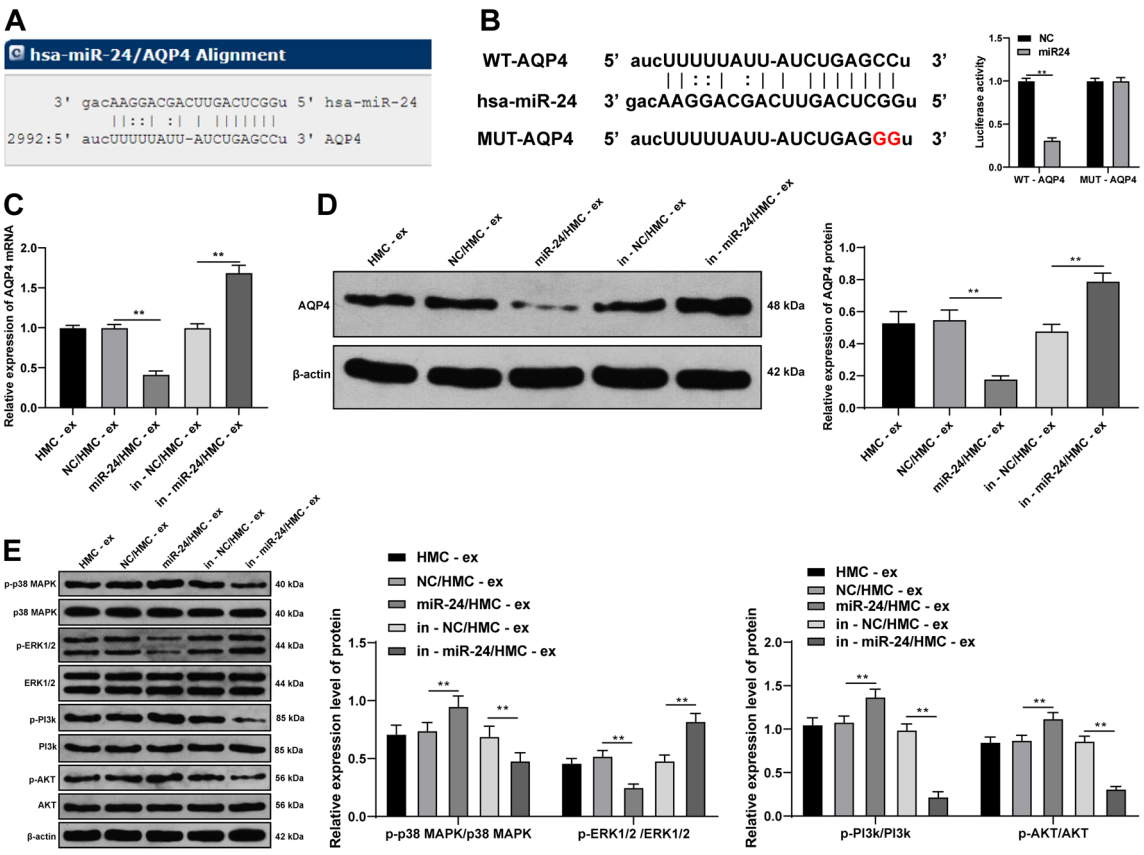

Fig. 4 miR-24 targets AQP4 to activate the P38 MAPK/ERK1/2/P13K/AKT axis. (**a**) The biological website predicted that the target gene of miR-24 contained AQP4; (**b**) Dual luciferase reporter gene assay precisely verified that there is a binding region between miR-24 and AQP4; (**c**) and (**d**) AQP4 levels in brain tissues of rats were detected by RT-qPCR and western blot analysis (n = 5); E. Western blot analysis was used to detect levels of P38 MAPK/ERK1/2/P13K/AKT signaling pathway-related proteins in the brain tissues of each rat (n = 5). The experiments were performed 3 times. *$p < 0.01$. Data in panels **c** and **d** were analyzed by one-way ANOVA, and data in panels **b** and **e** were analyzed by two-way ANOVA. Tukey's multiple comparisons test was used for pairwise comparison after ANOVA

the H/R injury model in SH-SY5Y cells. Specifically, we cultured human SH-SY5Y cells and treated them with different hypoxia time and then reperfusion for 24 h. We found that the apoptosis rate of SH-SY5Y cells was too high after 8 h of hypoxia while too low after 4 h. Therefore, we determined that the hypoxia time of H/R model at 6 h (Fig. 5a).

We cocultured the EVs derived from HMC-EVs with low- or over-expression of miR-24 with SH-SY5Y cells. Then we evaluated the effect of HMC-EVs with low- or over-expression of miR-24 on the activity of SH-SY5Y cells by MTT assay, colony formation assay and EdU staining, and evaluated the invasion and migration abilities by Transwell assay. The results showed that in the HMC-EV group with low/over expression of miR-24, the activity, and invasion and migration abilities of SH-SY5Y cells were significantly higher than those in the H/R group, while in the HMC-EV group with low expression of miR-24, the activity, invasion and migration ability of SH-SY5Y cells were significantly lower than those in the HMC-EV group (all $p < 0.05$) (Fig. 5b–e). Taken together, overexpression of miR-24 further promoted the recovery of SH-SY5Y cell proliferation ability after H/R injury, while HMC-EVs with low expression of miR-24 showed impaired effects.

Inhibition of the P38 MAPK/ERK1/2/P13K/AKT Axis Impairs the Recovery Effects of HMC-EVs-Carried miR-24 on SH-SY5Y Cell Proliferation and Invasion After H/R

To verify that HMC-EVs-carried miR-24 restored the proliferation and invasion of SH-SY5Y cells after H/R injury by regulating the P38 MAPK/ERK1/2 and P13K/AKT signaling pathway, we used LY294002 and PD98095 to inhibit the P38 MAPK/ERK1/2 and P13K/AKT signaling pathways. The results showed that the proliferation and invasion of SH-SY5Y cells treated with LY294002 and PD98095 was decreased significantly compared with SH-SY5Y

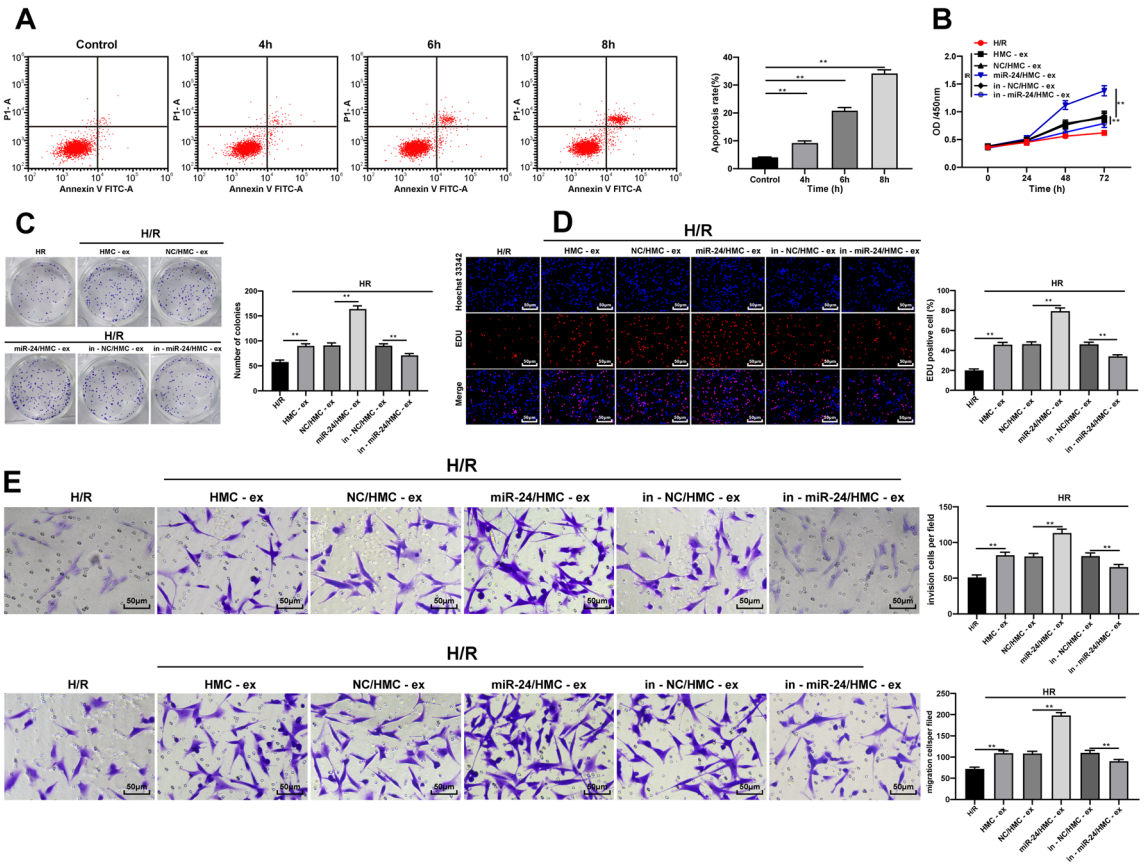

Fig. 5 HMC-EV-carried miR-24 restores SH-SY5Y cell proliferation and migration after H/R. (**a**) SH-SY5Y cell apoptosis after hypoxia was detected by flow cytometry; (**b**) SH-SY5Y cell activity at 0 h, 24 h, 48 h and 72 h was detected by MTT assay; C. SH-SY5Y cell colony formation ability was measured by cell colony formation assay; (**d**) EdU-positive cell in SH-SY5Y cells was measured by EdU labeling assay; E. SH-SY5Y cell invasion and migration ability was detected by Transwell assay. The experiments were performed 3 times. *$p < 0.01$. Data in panels **a**, **c**, **d** and **e** were analyzed by one-way ANOVA, and data in panel B were analyzed by two-way ANOVA. Tukey's multiple comparisons test was used for pairwise comparison after ANOVA

cells treated with overexpressing miR-24 in HMC-EVs (Fig. 6a–d).

Discussion

Stem cell therapy has a broad application prospect thanks to its capability in tissue repair and regeneration after IR [25]. Additionally, miRs are present in the blood after I/R, and circulating miRs may appear in EVs which stabilize miRs in plasma [14]. Inspired by these reviews, we performed this study with the aim to figure out the stem cell/miR combined therapy for cerebral I/R injury treatment. Collectively, we came to a conclusion that HMC-EVs-carried miR-24 played protective roles in cerebral I/R injury, possibly by targeting AQP4 and activating the P38 MAPK/ERK1/2/P13K/AKT pathway.

After HMC-EVs treatment, the infarct size, TUNEL-positive cells, Caspase-3 positive expression, and IL-6 and TNF-α levels were significantly lower than those in I/R rats. A former study noted that pulmonary dysfunction, lung injury, inflammation, edema and neutrophil infiltration after I/R were attenuated by MSC-derived EVs [7]. When I/R occurs, IL-6 expression increases as an effective early indicator of prognosis [2]. Interestingly, another study suggested that adipose MSC-derived EVs suppressed IL-1β, TNF-α, oxidative stress and cleaved Caspase-3, but increased Bcl-2 expression in liver I/R injury [26]. HMC-EVs injection reduced cardiac fibrosis and improved cardiac function in a rat model of acute myocardial infarction [27].

Through microarray analysis and RT-qPCR verification, we stated that miR-24 was differentially expressed in HMC-EVs and cerebral I/R injury rat tissues. Consistently, a recent study also found that miR-24 was noticeably downregulated in I/R through the profiling of miRs expression in a mouse model of renal IRI [28]. Furthermore, we performed a gain-and-loss of functions of miR-24 in HMC-EVs, and got a conclusion that miR-24 overexpression in HMC-EVs reduced cerebral I/R injury, while miR-24 knockdown in HMC-EVs impaired the protective roles of HMC-EVs in cerebral I/R injury. Similarly, miR-24-3p attenuated myocardial injury and reduced infarct size, Caspase-3 activity and TNF-α level by targeting receptor-interacting serine/threonine-protein kinase 1, thus exerting cardioprotective functions in myocardial IRI [29]. miR-24 was highly expressed in remote ischemic preconditioning-induced exosomes, and reduced oxidative stress-mediated injury and apoptosis, attenuated infarct size and improved heart function in myocardial I/R models [30]. To sum up, HMC-EVs could mitigate cerebral I/R injury by releasing miR-24.

Moreover, we noticed that HMC-EVs-carried miR-24 could target AQP4 to activate the MAPK/ERK1/2/P13K/AKT pathway, which further promoted the proliferation and migration of SH-SY5Y cells after H/R injury.

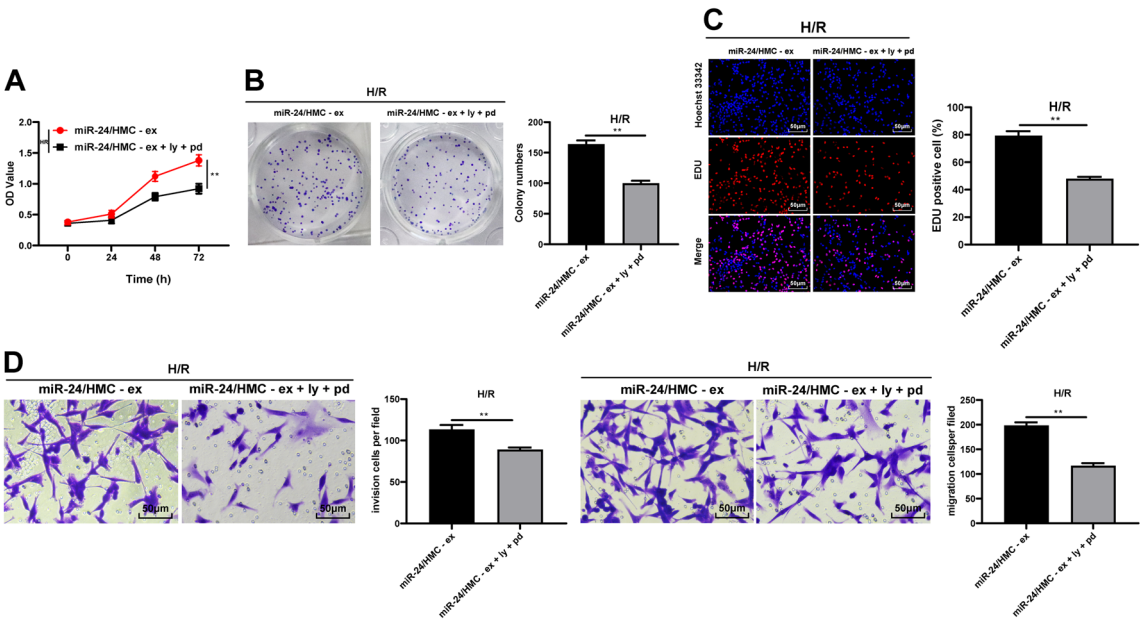

Fig. 6 Inhibition of the P38 MAPK/ERK1/2/P13K/AKT axis impairs the recovery effects of HMC-EV-carried miR-24 on SH-SY5Y cell proliferation and invasion after H/R. (**a**) SH-SY5Y cell activity at 0 h, 24 h, 48 h and 72 h was detected by MTT assay; (**b**) SH-SY5Y cell colony formation ability was measured by cell colony formation assay; (**c**) EdU-positive cell in SH-SY5Y cells was measured by EdU labeling assay; (**d**) SH-SY5Y cell invasion and migration ability was detected by Transwell assay. The experiments were performed 3 times. $^{*}p < 0.01$. Data in panels **b**, **c** and **d** were analyzed by the *t* test, and data in panel **a** were analyzed by two-way ANOVA. Tukey's multiple comparisons test was used for pairwise comparison after ANOVA

HMC-EVs can transfer RNA into injured renal tubular cells and change their gene expression, so as to promote cell dedifferentiation and regeneration, and finally improve tissue damage and organ disorder [31]. For example, Ranghino et al demonstrated that glomerular MSC-EVs ameliorated the impaired kidney functions after I/R injury by transferring mRNAs and miRs [32]. AQP4 is abundantly expressed in all brain structures and AQP4 alternation seems to parallel changes in neuroinflammation and cerebral edema [33, 34]. AQP4 was correlated with the maturation of blood–brain barrier, and was rapidly induced after ischemia coinciding with swelling of the ischemic hemisphere after stroke onset [35]. Importantly, AQP4 in astrocytes may aggravate cytotoxic brain edema after I/R by promoting water entry [4]. Of particular note, adipose MSC-EVs effectively suppressed immune-inflammatory responses and protected the brain from sepsis syndrome-induced damage by decreasing AQP4 levels [36].

MAPK pathway is involved in the regulation of inflammatory response, apoptosis and death in ischemic and hemorrhagic brain injury [37]. Transient and moderate ERK phosphorylation mediates cell protection during ischemic precondition [24]. Previous work showed that the PI3K/AKT may alleviate myocardial I/R injury [38]. Subsequently, we established the H/R injury model in SH-SY5Y cells, and added with LY294002 and PD98095, inhibitors of the P38 MAPK/ERK1/2 and P13K/AKT pathways, respectively. Inhibition of the P38 MAPK/ERK1/2/P13K/AKT axis impairs the recovery effects of HMC-EVs-carried miR-24 on SH-SY5Y cell proliferation and invasion after H/R. Another study has suggested that MSC-EVs increased myocardium viability and cardiac function, reduced infarct size and oxidative stress, and activated the PI3K/AKT pathway after I/R [39]. What's more, AKT-modified HMC-EV was reported to be effective for acute myocardial infarction treatment by improving cardiac function and promoting angiogenesis [40]. Moreover, Zhou et al. showed that HMC-EVs were able to repair acute kidney injury by improving oxidative stress, suppressing cell apoptosis, and promoting cell proliferation through activation of the ERK1/2 pathway [41].

Taken together, such a conclusion can be draw that the protective effects of HMC-EVs-carried miR-24 in cerebral I/R injury rat model and H/R cell model were achieved possibly by targeting AQP4 and activating the P38 MAPK/ERK1/2/P13K/AKT pathway. This study may provide novel insights for the understanding of I/R pathogenesis and treatment. Although miRs are now in clinical trials, stem cell-derived EVs need further investigations to translate its role in stem cell therapy. More researches are still needed to further validate our results and to verify the application values in clinic setting.

Data Availability All the data generated or analyzed during this study are included in this published article.

Compliance with Ethical Standards

Conflict of interest All authors declare that there is no conflict of interests in this study.

Ethics Approval This study was approved and supervised by the animal ethics committee of Qingdao Chengyang People's Hospital. Significant efforts were made to minimize the number of animals and their pain. All procedures were strictly conducted as per the Code of Ethics.

References

1. Kalogeris T, Baines CP, Krenz M et al (2012) Cell biology of ischemia/reperfusion injury. Int Rev Cell Mol Biol 298:229–317
2. Yang J, Chen M, Cao RY et al (2018) The role of circular RNAs in cerebral ischemic diseases: ischemic stroke and cerebral ischemia/reperfusion injury. Adv Exp Med Biol 1087:309–325
3. Wu MY, Yiang GT, Liao WT et al (2018) Current mechanistic concepts in ischemia and reperfusion injury. Cell Physiol Biochem 46:1650–1667
4. Nagy Z, Nardai S (2017) Cerebral ischemia/repefusion injury: from bench space to bedside. Brain Res Bull 134:30–37
5. Castro-Manrreza ME, Montesinos JJ (2015) Immunoregulation by mesenchymal stem cells: biological aspects and clinical applications. J Immunol Res 2015:394917
6. Li CY, Wu XY, Tong JB et al (2015) Comparative analysis of human mesenchymal stem cells from bone marrow and adipose tissue under xeno-free conditions for cell therapy. Stem Cell Res Ther 6:55
7. Stone ML, Zhao Y, Robert Smith J et al (2017) Mesenchymal stromal cell-derived extracellular vesicles attenuate lung ischemia-reperfusion injury and enhance reconditioning of donor lungs after circulatory death. Respir Res 18:212
8. Yan Y, Jiang W, Tan Y et al (2017) hucMSC exosome-derived GPX1 is required for the recovery of hepatic oxidant injury. Mol Ther 25:465–479
9. Cao H, Qian H, Xu W et al (2010) Mesenchymal stem cells derived from human umbilical cord ameliorate ischemia/reperfusion-induced acute renal failure in rats. Biotechnol Lett 32:725–732
10. Riazifar M, Pone EJ, Lotvall J et al (2017) Stem cell extracellular vesicles: extended messages of regeneration. Annu Rev Pharmacol Toxicol 57:125–154
11. Shen B, Liu J, Zhang F et al (2016) CCR2 positive exosome released by mesenchymal stem cells suppresses macrophage functions and alleviates ischemia/reperfusion-induced renal injury. Stem Cells Int 2016:1240301
12. Barile L, Moccetti T, Marban E et al (2017) Roles of exosomes in cardioprotection. Eur Heart J 38:1372–1379
13. Turturici G, Tinnirello R, Sconzo G et al (2014) Extracellular membrane vesicles as a mechanism of cell-to-cell communication: advantages and disadvantages. Am J Physiol Cell Physiol 306:C621–C633
14. Kalogeris T, Baines CP, Krenz M et al (2016) Ischemia/reperfusion. Compr Physiol 7:113–170
15. Zhang B, Shen L, Shi H et al (2016) Exosomes from human umbilical cord mesenchymal stem cells: identification, purification, and biological characteristics. Stem Cells Int 2016:1929536

16. Longa EZ, Weinstein PR, Carlson S et al (1989) Reversible middle cerebral artery occlusion without craniectomy in rats. Stroke 20:84–91
17. Bederson JB, Pitts LH, Tsuji M et al (1986) Rat middle cerebral artery occlusion: evaluation of the model and development of a neurologic examination. Stroke 17:472–476
18. Kan S, Zhou H, Jin C et al (2015) Effects of PDTC on NF-kappaB expression and apoptosis in rats with severe acute pancreatitis-associated lung injury. Int J Clin Exp Med 8:3258–3270
19. Chen C, Meng Q, Xia Y et al (2018) The transcription factor POU3F2 regulates a gene coexpression network in brain tissue from patients with psychiatric disorders. Sci Transl Med 10
20. Thery C, Witwer KW, Aikawa E et al (2018) Minimal information for studies of extracellular vesicles 2018 (MISEV2018): a position statement of the International Society for Extracellular Vesicles and update of the MISEV2014 guidelines. J Extracell Vesicles 7:1535750
21. Vicencio JM, Yellon DM, Sivaraman V et al (2015) Plasma exosomes protect the myocardium from ischemia-reperfusion injury. J Am Coll Cardiol 65:1525–1536
22. Chiba M, Kimura M, Asari S (2012) Exosomes secreted from human colorectal cancer cell lines contain mRNAs, microRNAs and natural antisense RNAs, that can transfer into the human hepatoma HepG2 and lung cancer A549 cell lines. Oncol Rep 28:1551–1558
23. Zheng Y, Pan C, Chen M et al (2019) miR29a ameliorates ischemic injury of astrocytes in vitro by targeting the water channel protein aquaporin 4. Oncol Rep 41:1707–1717
24. Zhou J, Du T, Li B et al (2015) Crosstalk between MAPK/ERK and PI3K/AKT signal pathways during brain ischemia/reperfusion. ASN Neuro 7
25. Prathipati P, Nandi SS, Mishra PK (2017) Stem cell-derived exosomes, autophagy, extracellular matrix turnover, and miRNAs in cardiac regeneration during stem cell therapy. Stem Cell Rev Rep 13:79–91
26. Sun CK, Chen CH, Chang CL et al (2017) Melatonin treatment enhances therapeutic effects of exosomes against acute liver ischemia-reperfusion injury. Am J Transl Res 9:1543–1560
27. Yaghoubi Y, Movassaghpour A, Zamani M et al (2019) Human umbilical cord mesenchymal stem cells derived-exosomes in diseases treatment. Life Sci 233:116733
28. Zhang L, Song Y, Chen L et al (2019) MiR-20a-containing exosomes from umbilical cord mesenchymal stem cells alleviates liver ischemia/reperfusion injury. J Cell Physiol
29. Tan H, Qi J, Fan BY et al (2018) MicroRNA-24-3p attenuates myocardial ischemia/reperfusion injury by suppressing RIPK1 expression in mice. Cell Physiol Biochem 51:46–62
30. Minghua W, Zhijian G, Chahua H et al (2018) Plasma exosomes induced by remote ischaemic preconditioning attenuate myocardial ischaemia/reperfusion injury by transferring miR-24. Cell Death Dis 9:320
31. Ju GQ, Cheng J, Zhong L et al (2015) Microvesicles derived from human umbilical cord mesenchymal stem cells facilitate tubular epithelial cell dedifferentiation and growth via hepatocyte growth factor induction. PLoS One 10:e0121534
32. Ranghino A, Bruno S, Bussolati B et al (2017) The effects of glomerular and tubular renal progenitors and derived extracellular vesicles on recovery from acute kidney injury. Stem Cell Res Ther 8:24
33. Clement T, Rodriguez-Grande B, Badaut J (2020) Aquaporins in brain edema. J Neurosci Res 98:9–18
34. Fukuda AM, Badaut J (2012) Aquaporin 4: a player in cerebral edema and neuroinflammation. J Neuroinflammation 9:279
35. Hirt L, Ternon B, Price M et al (2009) Protective role of early aquaporin 4 induction against postischemic edema formation. J Cereb Blood Flow Metab 29:423–433
36. Chang CL, Chen HH, Chen KH et al (2019) Adipose-derived mesenchymal stem cell-derived exosomes markedly protected the brain against sepsis syndrome induced injury in rat. Am J Transl Res 11:3955–3971
37. Sun J, Nan G (2016) The mitogen-activated protein kinase (MAPK) signaling pathway as a discovery target in stroke. J Mol Neurosci 59:90–98
38. Zhao MM, Yang JY, Wang XB et al (2013) The PI3K/Akt pathway mediates the protection of SO(2) preconditioning against myocardial ischemia/reperfusion injury in rats. Acta Pharmacol Sin 34:501–506
39. Arslan F, Lai RC, Smeets MB et al (2013) Mesenchymal stem cell-derived exosomes increase ATP levels, decrease oxidative stress and activate PI3K/Akt pathway to enhance myocardial viability and prevent adverse remodeling after myocardial ischemia/reperfusion injury. Stem Cell Res 10:301–312
40. Ma J, Zhao Y, Sun L et al (2017) Exosomes derived from Akt-modified human umbilical cord mesenchymal stem cells improve cardiac regeneration and promote angiogenesis via activating platelet-derived growth factor D. Stem Cells Transl Med 6:51–59
41. Zhou Y, Xu H, Xu W et al (2013) Exosomes released by human umbilical cord mesenchymal stem cells protect against cisplatin-induced renal oxidative stress and apoptosis in vivo and in vitro. Stem Cell Res Ther 4:34